

## Research papers

# Performance and economic analysis of steam extraction for energy storage to molten salt with coupled ejector and thermal power units

Xiang Liu, Kelang Jin, Xue Xue, Lei Zhang, Hao Zhou\*

Zhejiang University, Institute for Thermal Power Engineering, State Key Laboratory of Clean Energy Utilization, Hangzhou 310027, PR China



## ARTICLE INFO

## Keywords:

Steam extraction  
Ejector  
Thermal power flexibility  
Exergy loss  
Economic analysis

## ABSTRACT

A new thermal power unit peaking system coupled with thermal energy storage and steam ejector was proposed, which is proved to be technically and economically feasible based on the simulation of a 600 MW thermal power unit. Results show that the percentage of exergy losses in the retrofitted system is in the order of condenser, turbine and thermal energy storage system, with the exergy losses in the heat release process accounting for approximately 70 % of the cycle. The condenser and evaporator corresponding to the storage and heat processes account for 60 % of the total exergy losses in thermal energy storage system. The retrofitted system has a maximum cycle efficiency of 70–80 % with low and peak modulation rates of 16.5 % and 11.7 %. Extraction of main steam dominates the peaking rate and cycling efficiency compared to extraction of reheat steam. Increasing the main steam pressure at the ejector inlet increases the low peaking rates by 1.5 %, while reducing the molten salt flow rate per unit peaking depth by 10 t/h, which is essential for the stable operation of the retrofitted system. The economic analysis of the retrofitted system shows that the system operating time is the main factor affecting the payback period compared to the interest rate and starts to be profitable in 3.8 years, with later profitability of up to RMB 25 million/year. Further analysis reveals that two different extractions of reheat steam with the same extraction of main steam will achieve the same payback period, which offers a variety of possibilities for practical operational scenarios. In addition, when the extraction of main steam is <250 t/h, the payback time of the system will exceed 15 years, at which point it will be challenging to meet the economic viability of the retrofitted system.

Increasing emission of greenhouse gases is causing irreversible damage to the global ecological environment with the progress of industrialization and urbanization worldwide. New energy power is the future of energy because of clean, non-polluting and widely available [1,2]. According to the International Energy Agency, the grid connection rate of renewable energy sources has gone from 18.5 % to 28.6 % in 20 years [3]. 95 % of new electricity capacity in the next 30 years will be renewable, with solar and wind power accounting for 90 % of this [4]. However, wind and solar power have strong volatility and anti-peak characteristics, posing a huge challenge to grid peaking [5,6]. At present, thermal power is mature and has serious overcapacity, and more and more thermal power units need to maintain low-load operation for long periods. In this context, how to further enhance the dispatch ability of thermal power units has become the focus of grid regulation. More flexible plants can help the market accommodate more renewable energy and promote low carbon emissions [7,8].

Currently, steam cycle is the main power generation method for nuclear and thermal power units, and thermal energy storage (TES)

technology has been a hot research topic in recent years [9,10]. The TES and steam cycle combination is a powerful means to improve grid flexibility. Stevanovic et al. [11] found that the coupling of TES with thermal power units could further enhance unit flexibility, with steam generated by the boiler not being introduced into the turbine but absorbed using the energy storage medium, solving the problem of supply and demand imbalance during low periods. Kindi et al. [12] found that the addition of TES and secondary generator systems could result in annual savings of \$28.5 to \$104.3 million in nuclear power system costs when studying the optimal dispatch of nuclear power plants. A report from Saarland, Germany [13] noted that high-temperature latent heat TES units in CHP plants could provide steam and electricity to customers in emergencies, alleviating the city's thermo-electric coupling problem.

Similarly, data from power plants in Germany and Austria [14,15] show that transferring steam energy to molten salt and water can achieve storage capacities of up to 1000 MWh, much higher than the working capacity and operating time of steam energy storage. Further,

\* Corresponding author.

E-mail address: [zhouhao@zju.edu.cn](mailto:zhouhao@zju.edu.cn) (H. Zhou).

### Nomenclature

EMS	extraction of main steam
ITMS	molten salt temperature after the first heat exchange stage
ME	molten salt heat exchangers
NPV	net present value
SJP	steam jet pump
TPSE	steam ejector to couple the TES and the thermal power unit (retrofitted system)
ERS	extraction of reheat steam
LVR	low valley regulation rate
MSFR	molten salt flow rate variation
PMR	peak modulation ratio
TES	thermal energy storage

several scholars have investigated different strategies for extracting steam combinations after coupling TES to thermal power units. Li et al. [16] proposed three HTTS charging strategies and two HTTS discharging strategies, which were tested by a simulation platform. The simulation results showed that extracting steam from the turbine to charge the HTTS and discharge the stored thermal energy back into the power generation process is feasible. Jacek D et al. [17,18] conducted a technical feasibility study for integrating TES into a 375mw sub-critical oil-fired conventional power plant and evaluated the optimal heat extraction candidates for the TES charging and discharging processes. The results showed that integrating TES into the power plant cycle is feasible and highly efficient.

An ejector, also known as a steam jet pump (SJP), is a flow device with two inlets for high and low pressure and a discharge port for medium pressure. Thermal and nuclear power systems often use main steam or reheated steam as the high-pressure stream and direct the low-pressure extracted or exhausted steam from the turbine as the heat source, which has good industrial application prospects and strong technical feasibility. Xue et al. [19] coupled a thermal power unit and desalination system based on an adjustable steam ejector, achieving good benefits. Zhang et al. [20] studied a thermoelectric system with a  $2 \times 350$  MW thermal power unit coupled with a steam ejector and used the main steam induced discharge steam to provide the heat source to improve the waste heat recovery rate by 8.66 %. Peng et al. [21] used an ejector to couple ORC and low-temperature geothermal energy and analyzed the effect of different heat source temperatures on the power generation performance of the system.

In order to ensure system economy while further improving the flexibility of thermal power units, the operating mode of a new thermal power unit coupled to a TES needs to be further investigated. This work introduces a steam ejector to couple the TES and the thermal power unit (TPSE) by extracting main steam and reheating steam for thermal storage during low periods. The high and low-pressure inlets of the steam ejector are the main steam and reheat steam after the heat exchange. Medium-pressure steam from the outlet go to the cold inlet of the reheater which ensures the inlet steam flow meets the minimum load of the turbine. This new peaking strategy for thermal power units will allow the system to have deep peaking capability while ensuring very high thermal efficiency. Using a 600 MW thermal power unit as a reference, the multi-state heat balance diagram of TPSE is calculated on the basis of self-programming software to study the specific effects of the extraction flow distribution, the inlet pressure, ejector coefficient and the internal parameters of the TES on TPSE. In addition, the economic benefits and cost analysis of TPSE are calculated by the net present value (NPV) method to provide new ideas and references for improving the deep peaking capacity of thermal power units.

## 1. Introduction to the TPSE system

The TPSE system is shown in Fig. 1. The whole system has two parts, the upper part is the original thermal unit in operation and contains the steam boiler (1), heat exchanger (2), turbine (3), generator (4), deaerator (5) and condenser (6). In addition, points 1 and 2 indicate shaft seal leaks going to the deaerator and condenser outlets for heating condensate, respectively, and A to F indicate the flow stock interface of the TES with the original thermal unit. The lower section is the added TES and steam generation systems (SGS), including cold salt tank (7), hot salt tank (8), superheater or subcoolers (9), evaporator or condenser (10), pre-heater (11), three-way valve gate (12), steam ejector (13), where (9) (10) (11) are all molten salt heat exchangers (ME). During the low power peak period, part of the main steam and reheat section steam is extracted, and the heat is stored in the TES with molten salt as the medium, and the storage capacity is to meet the requirements of peak regulation for >6 h. Three sets of ME are installed in the TES, two of which are used to store the heat of the main steam and one to store the heat of the reheat steam. The cold salt is divided by a valve at the storage tank outlet into two streams, one for heat exchange with the main steam in order and one for heat exchange with the reheat steam. The heat exchange of the main steam is divided into two stages, the first being the super-cooler, which converts the main steam from high-temperature superheated steam to medium-temperature superheated steam; the second stage is the condenser, which converts the main steam from superheated steam to unsaturated water and introduces it to the boiler make-up water. The reheated steam is direct heat exchanged with the cold salt and remains as superheated steam. The high-pressure inlet of the steam ejector is the main steam after the first heat exchange stage, and the low-pressure inlet is the reheated steam after the heat exchange. The two are fully mixed in the ejector to make the pressure and temperature of the steam meet the requirements of the cold end parameters of the reheater, which ensure the safe and stable operation of the boiler. The molten salt absorbs the heat from the steam and returns to the hot salt tank, thus completing the heat storage process. During low periods, the heat is stored in the TES and used to heat the feed water from the deaerator, producing superheated steam that is returned to the cold section of the reheater during peak periods. After reheating, it is warmed up and returned to the medium-pressure cylinder to do work, increasing the output of the unit. The entire SGS consists of a pre-heater, evaporator and superheater.

## 2. Mathematical models

$C\#$  was used to build the set of TPSE models, including the thermal unit model, the steam ejector model, the TES system model and the main economic indicators.

### 2.1. Thermal power unit model

The thermal power unit system mainly consists of steam boiler, steam turbine, high and low-temperature heat exchanger, etc. The variable working process of the turbine system is calculated according to Freugel's formula [22]. Where  $q$ ,  $p$  and  $T$  denote steam mass flow, pressure and temperature, 1 and 0 denote variable and base conditions, respectively, and  $i$  and  $o$  denote pre-stage and post-stage.

$$\frac{q_1}{q_0} = \sqrt{\frac{p_{i,1}^2 - p_{o,1}^2}{p_{i,0}^2 - p_{o,0}^2}} \times \sqrt{\frac{T_0}{T_1}} \quad (1)$$

The core of high and low-temperature heat exchangers is energy conversion, the heat exchange process of hot and cold fluids follows the energy conservation law. Where  $h$  denotes specific enthalpy, J/kg;  $\eta_{\text{heater}}$  denotes heat transfer efficiency,  $c$  and  $h$  denote hot and cold fluids, and out and in denote heat exchanger inlet and outlet.

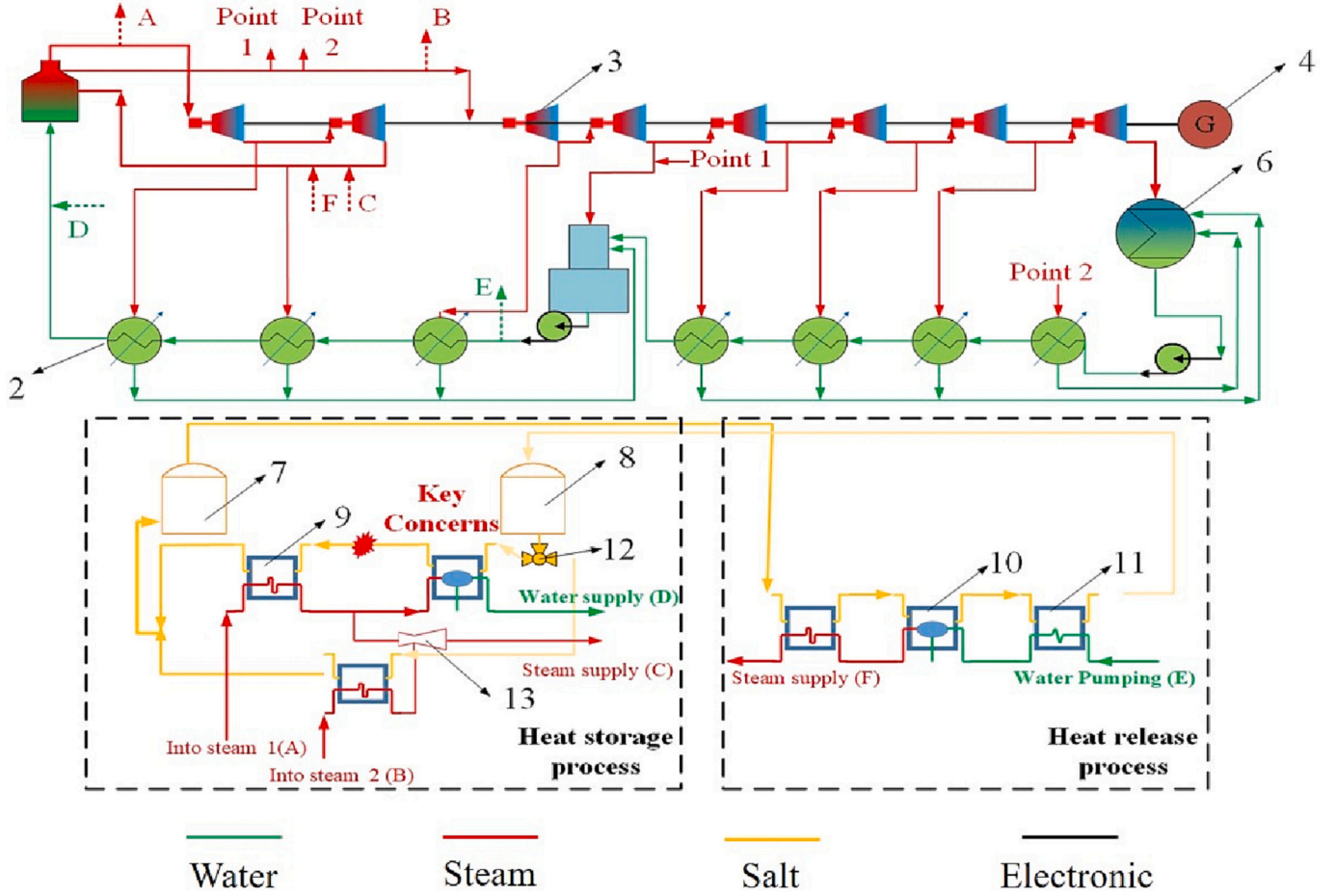


Fig. 1. Flow chart of the TPSE system.

$$q_c(h_{c,out} - h_{c,in}) = q_h(h_{h,in} - h_{h,out})\eta_{heater} \quad (2)$$

## 2.2. TES model

Currently, most large molten salt TES plants use a double-tank heat storage system. Therefore, a double-tank model has been chosen for the built-in process of this work. Molten salt is used as a medium for heat transfer and storage, but the freezing point of molten salt is relatively high and measures such as insulation and electrical heating of the molten salt tank are required to prevent the molten salt from solidifying. For a two-tank molten salt TES system, the minimum amount of energy that needs to be stored in the molten salt tank, the mass of molten salt required and the design volume of the molten salt tank can be derived from the heat balance of the TES-coupled thermal unit in a peaking cycle.

$$M = \frac{Q_1}{C_p T_{h-c}} \quad V = \frac{M}{\lambda \rho} \quad (3)$$

where  $Q_1$  is the energy required to be stored in the system during a peaking cycle, J;  $C_p$  is the specific heat capacity of the molten salt, J/kg K;  $T_{h-c}$  is the temperature difference between the hot and cold salt, °C;  $M$  is the mass of molten salt required for the system,  $\rho$  is the density of the molten salt and  $\lambda$  is the safety factor when considering the thermal expansion and contraction of the fluid as well as the actual manufacturing situation;  $V$  is the molten salt tank capacity.

## 2.3. Steam ejector model

The steam ejector structure is shown in Fig. 2. The mixing chamber, mixing chamber throat and pressure expansion tube are the main structures of the ejector, with the nozzle in the mixing chamber being the focus of the entire system. There are three fluids in the steam ejector, the high-pressure working fluid, which is the main steam after the first heat transfer; the low-pressure induced fluid, which is the reheat steam; and the mixing fluid, which is the medium at the exit of the steam ejector going to the cold section of the reheater. To simplify the model, the following assumptions are made in the steam ejector modeling: (1) the steam ejector works under critical conditions; (2) fluid flow is an adiabatic process; (3) the working fluid and the induced fluid in the mixing chamber complete isobaric mixing. Since steam ejector performance has a significant impact on the overall economy of the system, the injection coefficient  $\beta$  is usually used to measure the performance of steam ejectors [23] and is expressed as Eq. (4).

$$\beta = q_s/q_p \quad (4)$$

where:  $q_s$  is the mass flow rate of the fluid being induced;  $q_p$  is the mass flow rate of the working fluid. In the mixing process, the fluid follows the laws of mass conservation, momentum conservation and energy conservation, expressed as Eq. (5) [24].

$$\begin{aligned} (q_{m,p}v_{p-y} + q_{m,s}v_{s-y})\varphi_m &= (q_{m,s} + q_{m,p})v_m \\ q_{m,p}\left(\frac{v_{p-y}^2}{2} + h_{p-y}\right) + q_{m,s}\left(\frac{v_{s-y}^2}{2} + h_{s-y}\right) &= \\ (q_{m,s} + q_{m,p})\left(\frac{v_m^2}{2} + h_m\right) & \end{aligned} \quad (5)$$

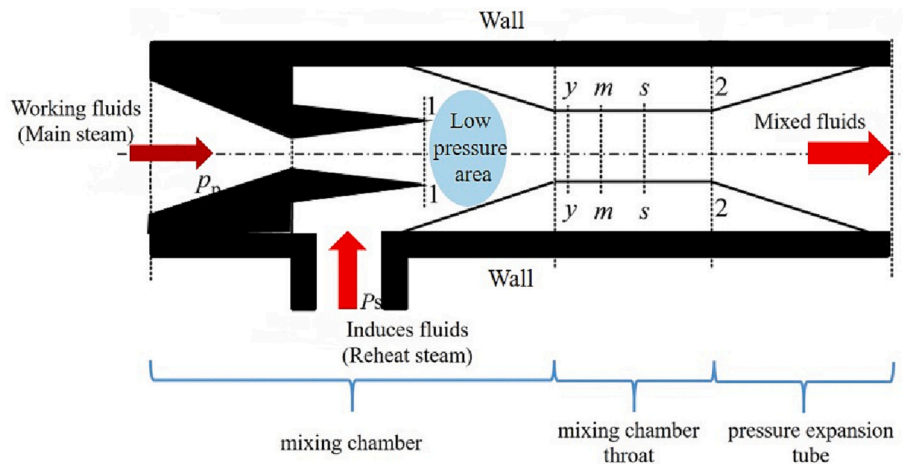


Fig. 2. Construction of steam ejector [24].

where the combined subscripts shaped as (a, b) within a represents the cross-sectional position and b represents the fluid type. Where s represents the induced fluid, and the cross-sectional positions are numbered as shown in Fig. 3.  $v$  represents the flow velocity,  $m/s$ , and  $\phi$  represents the momentum loss coefficient during fluid mixing.

The mixed fluid generates a surge at the s-s section, where the flow velocity decreases and the pressure rises rapidly, satisfying the following series of equations before and after the surge [24].

$$\begin{aligned}
 a_m &= f(p_m, h_m) \\
 \gamma_m &= g(p_m, h_m) \\
 Ma_m &= v_m/a_m \\
 p_2 &= p_m \left[ 1 + \frac{2\gamma_m}{\gamma_m + 1} (Ma_m^2 - 1) \right]
 \end{aligned}
 \tag{6}$$

where:  $a_m$  is the speed of sound of the mixed fluid at the m-m cross-section;  $\gamma_m$  is the isentropic exponent of the mixed fluid at the m-m cross-section;  $Ma_m$  is the Mach number of the mixed fluid at the m-m cross-section;  $f$  and  $g$  are both physical functions;  $p_2$  is the pressure of the mixed fluid at the inlet of the diffuser 2-2. The mixed fluid is decelerated and pressurized through the diffuser, and the enthalpy at the ejector

outlet is  $h_B$ , which can be obtained according to the energy conservation law [24].

$$h_B = h_m + v_m^2/2 \tag{7}$$

### 2.4. Key evaluation indicators for TPSE

#### 2.4.1. Exergy analysis

Numerous research has shown that exergy analysis is an effective method for assessing the impact of TES and steam ejectors on thermal power systems, providing the right direction for improving the performance of coupled systems [25].

$$E_f = q_f [h_f - h_0 - T_0 (s_f - s_0)] \tag{8}$$

where  $E_f$  is the exergy flow of the working fluid, kW;  $q_f$  is the mass flow of the working fluid, kg/s;  $h_f$  is the specific enthalpy of the working fluid, kJ/kg;  $s_f$  is the specific entropy of the working fluid, kJ/(kg·K);  $h_0$  and  $s_0$  are the specific enthalpy and entropy of the working fluid at the reference pressure (0.1 MPa) and temperature (273 K), kJ/kg, kJ/(kg·K). For a complete thermal system [25], the exergy balance equation is Eq. (9), where  $E_{in}$  and  $E_{out}$  are the exergy flow of the working fluid entering and

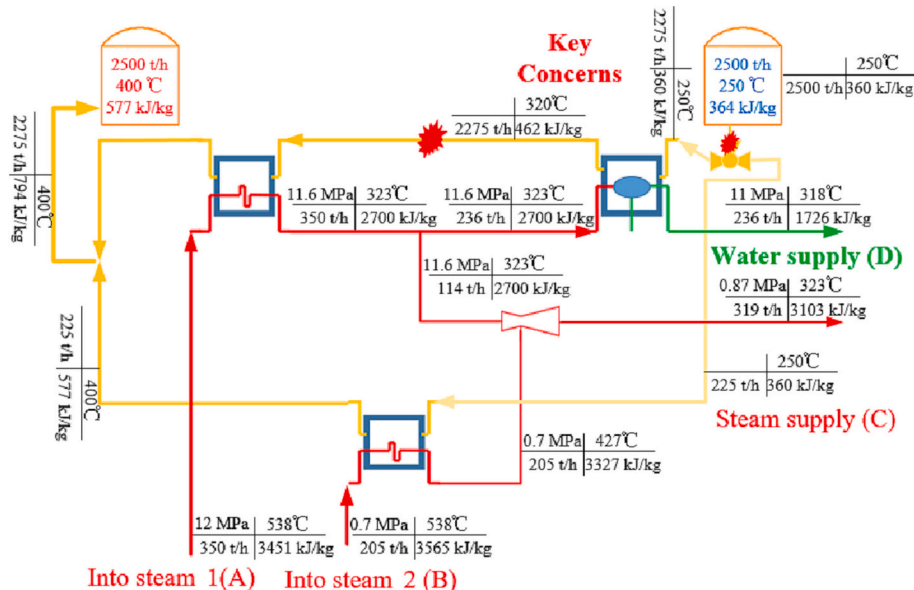


Fig. 3. Main parameters of the thermal storage process.

leaving the thermal system, kW;  $E_{\text{loss}}$  is the exergy loss of the thermal system, kW;  $E_t$  is the power generated by the turbine, kW.

$$\sum E_{\text{in}} = \sum E_{\text{out}} + \sum \text{loss} + E_t \quad (9)$$

#### 2.4.2. Peaking indicators

The maximum and minimum power output of the original thermal power unit is  $P_{\text{max1}}$  and  $P_{\text{min1}}$ , and the maximum and minimum power output of the TPSE is  $P_{\text{max2}}$  and  $P_{\text{min2}}$ , respectively. During low and peak power periods, TPSE has  $d_{\text{max}}$  and  $d_{\text{min}}$  compared to the original unit as the low valley regulation rate and peak modulation ratio (LVR and PMR), calculated as in Eq. (10), and  $P_E$  is the rated output power, taken 600 MW in this paper.

$$d_{\text{max}} = \frac{P_{\text{max2}} - P_{\text{max1}}}{P_E} \times 100\% \quad d_{\text{min}} = \frac{P_{\text{min1}} - P_{\text{min2}}}{P_E} \times 100\% \quad (10)$$

In order to describe the overall efficiency of the TES system in the heat storage and release process, this work introduces cycle efficiency as an essential indicator to determine the impact of TES on the system [26], calculated as in Eq. (11).

$$\eta_{\text{cycle}} = \frac{P_{\text{max2}} - P_{\text{max1}}}{P_{\text{min1}} - P_{\text{min2}}} \times 100\% \quad (11)$$

The introduction of molten salt flow per unit peaking depth describes the relationship between the TES system and thermal power units, clarifies the extent to which molten salt flow affects the peaking depth of the system, and compares the peaking difficulty of the TPSE under different operating conditions. Where  $q_{\text{unit}}$  is the unit peak molten salt flow rate, t/h;  $M_{\text{sto1}}$  indicates the mass of main steam extracted from the thermal storage process, t/h;  $M_{\text{sto2}}$  indicates the mass of reheat steam extracted from the thermal storage process;  $H_{\text{ext1}}$  and  $H_{\text{exh1}}$  indicate the enthalpy of extraction and the enthalpy of discharge of main steam, kJ/kg;  $H_{\text{ext2}}$  and  $H_{\text{exh2}}$  indicate the enthalpy of extraction and the enthalpy of discharge of reheat steam, kJ/kg. It is worth noting that the main steam and reheated steam discharge go to condensate and superheated steam, which must be calculated separately.  $C_p$  indicates the specific heat capacity of the molten salt, kJ/(kg·°C);  $t_2$  and  $t_1$  are the temperatures of the hot and cold molten salt, respectively, °C.

$$q_{\text{unit}} = \frac{M_{\text{sto1}}(h_{\text{ext1}} - h_{\text{exh1}}) + M_{\text{sto2}}(h_{\text{ext2}} - h_{\text{exh2}})}{100d_{\text{min}}c_p(t_2 - t_1)} \quad (12)$$

#### 2.4.3. Thermal power unit indicators

The heat consumption rate of a power unit is the ratio of the heat value of fuel consumed per hour to the amount of electricity generated [27], expressed in kJ/kWh, which reflects the efficiency of the unit in converting the heat energy in the fuel into electricity. At present, the assessment and analysis of the heat consumption rate index have been generally valued by power plants and have become one of the essential means of monitoring the operation of power plant systems. Calculated as in Eq. (13) where  $M_1$  and  $M_2$  are the main steam and reheat steam flows respectively, t/h;  $h_{\text{water}}$  indicates the enthalpy of the boiler feed water, kJ/kg;  $h_{\text{cold}}$  indicates the enthalpy of the cold section of reheat steam, kJ/kg;  $P$  is the system power generation at this time, MW.

$$\zeta = \frac{M_1(h_{\text{ext1}} - h_{\text{water}}) + M_2(h_{\text{ext2}} - h_{\text{cold}})}{P} \quad (13)$$

$\zeta$  is a description of the operating efficiency of the system. To further clarify the operating cost of the system, this work further calculates the coal consumption, t/h, to facilitate a comparison of the system under different operating conditions. Where  $M_{\text{coal}}$  is the standard coal consumption rate, t/h;  $Q_{\text{coal}}$  is the standard coal heat content, kJ/t;  $\eta_p$  is the pipeline efficiency, taken as 99%;  $\eta_b$  is the boiler efficiency, taken as 93.5%.

$$M_{\text{coal}} = \frac{\xi}{Q_{\text{coal}}\eta_p\eta_b} \quad (14)$$

#### 2.4.4. System economic indicators

To explain the superiority of TPSE, this work compares the economics of TPSE with that of the original thermal units. TPSE stores steam energy in the TES during low periods and releases heat to the grid during peak periods, further increasing the additional power output of the unit, at which time the tariff is higher and needs to be increased from the average tariff to be traded. Therefore, the expression for the economics of TPSE compared to the original thermal unit is shown in Eq. (15), with  $C_{\text{cycle}}$  being the difference in revenue between TPSE and the original thermal unit over 1 cycle, i.e. one day;  $u$  is the discount factor introduced to take into account the difference in economical price between peak and valley power, and  $H$  is the number of peaking hours in 1 cycle. When  $C_{\text{cycle}} > 0$ , TPSE starts the cycle at a profit and the opposite is true for a loss. It is worth pointing out that profitability here is not the start of positive returns for the whole system, the true accounting should also consider system modifications, TES and associated investment costs, and the existence of payback years, the details of which are described in Section 3.4.

$$C_{\text{cycle}} = H[(1+u)(P_{\text{max2}} - P_{\text{max1}}) + (1-u)(P_{\text{min2}} - P_{\text{min1}})] \quad (15)$$

#### 2.5. Model validation

Using a thermal power unit with a design rating of 600 MW as a reference, the unit design parameters were input into the program created in this work to verify the correctness of the mathematical model created for the thermal power unit. The mechanical efficiency of the device is taken as 95%, the generator efficiency of the device as 99% and the TES charging and discharging efficiency as 92%. It can be seen that the mathematical model developed in this work can calculate the operating parameters of thermal power units very well, and the errors between the calculated values of the model and the actual design values are within 0.5%. Therefore, the authors conclude that the mathematical model developed in this work has high accuracy and is fully capable of calculating complex thermal power unit systems. In order to verify the accuracy of the coupled energy storage module calculations, this work compares the heat exchanged between the molten salt side and the vapor side under Case3 thermal storage condition, as shown in the lower part of Table 1. The heat exchanged fully satisfies the given efficiency, which verifies the accuracy of the energy storage model. In addition, the mass balance is simpler and will not be verified separately. Later calculations related to coupled TES and steam ejectors are based on this mathematical model.

### 3. Results and discussion

#### 3.1. Analysis of baseline operating conditions

A 600 MW thermal power unit was selected as the experimental system for this work. A sub-critical unit has seven stages of heat recovery steam extraction, including three high-pressure heaters, three low-pressure heaters and a deaerator. The steam for energy storage comes from the main steam and reheated steam. The original unit was designed for 22% of the rated power for pure condensing conditions, the rated pressure of the unit's main steam was 16.7 MPa, the rated main steam temperature was 538 °C, the rated steam intake was 1845 t/h, the rated discharge pressure was 16 kPa and the boiler feedwater temperature was 278.6 °C.

To further clarify the specific operating conditions of the TPSE, the following four basic operating cases were analyzed: Case 1 is the rated operating output of 600 MW; Case 2 is the design minimum condensate operating condition with a design output of 130 MW; Case 3 is the heat storage condition based on Case 2, the steam extraction and storage mode of the TPSE, with design turbine output and storage power of 30 MW and 100 MW respectively; Case 4 is the heat release condition based

**Table 1**  
Comparison of the main parameters of the designed and built models.

Comparison	22%THA			100%THA		
	Design	Model	Error %	Design	Model	Error %
Power KW	130,239	130,553	0.24	600,000	600,242	0.04
Main steam t/h	420	420	0.00	1845	1845	0.00
Main steam temperature °C	538	538	0.00	538	538	0.00
Main steam pressure MPa	11.9	11.9	0.00	16.7	16.7	0.00
Reheat steam flow t/h	382.6	381.8	0.21	1580.6	1578	0.16
Reheat steam temperature °C	538	538	0.00	538	538	0.00
Reheat steam pressure MPa	0.86	0.86	0.00	3.879	3.88	0.026
Waste steam flow t/h	329.14	328.8	0.1	1356.3	1363	0.49
Waste steam temperature °C	54.34	54.16	0.33	55.31	55.31	0.00
Waste steam specific enthalpy kJ/kg	2600.3	2600	0.011	2435.8	2436	0.008

Heat exchange in TES	Molten salt side	Water and steam side	Setting efficiency	Actual efficiency
kJ	$5.32 \times 10^8$	$5.41 \times 10^8$	98 %	98 %

on Case 1, the steam generation mode of the TPSE, with design turbine output and additional boost power of 600 MW and 100 MW respectively. It is worth noting that energy storage and extra power are ideal conditions, and there must be losses in actual operation, which will be discussed further below. Cases 1 and 2 are the operating conditions of the original thermal unit, and the main operating parameters of the two conditions are given in Table 1. As such thermal units are more common, no further analyses were made in this work. The following analysis focuses on the energy storage and release conditions of the TPSE, Cases 3 and 4.

The main steam and reheat steam provides the energy storage mode for Case 3 as shown in Fig. 4. 350 t/h and 205 t/h of main steam and reheat steam are extracted respectively, both at a temperature of 538 °C. The cold salt tank discharges 2500 t/h of cold salt at 250 °C and is diverted by a three-way valve to the condenser and ME2 to absorb the heat from the main steam and reheat steam, with the cold salt and main steam in a counter flow arrangement. As shown in Fig. 4, 225 t/h and 2275 t/h of cold salt are first sent to the ME2 and condenser. At this point, the main steam in the condenser has completed the first heat exchange stage with the molten salt in ME1. After the first stage of heat exchange, the pressure of the main steam drops to 11.6 MPa, and the

temperature drops to 323 °C, while the temperature of the reheated steam drops to 427 °C. Case 3 sets the steam ejector injection coefficient at 1.8. Based on the reheat steam flow rate, the required high-pressure main steam is 114 t/h. Therefore, 319 t/h, 0.87 MPa, 323 °C of mixed steam flow towards the cold end of the reheat steam from the ejector outlet, adding steam to the reheat boiler to meet the minimum operating load of the boiler. The molten salt in the condenser is heated to 400 °C by the remaining main steam and returned to the hot salt tank, where the main steam condenses and supplies the boiler with water. Thus, the energy extracted is partially stored in the molten salt, and the remaining energy is returned to the boiler in the form of superheated steam and condensate to ensure the safe operation of the boiler. The output power is reduced from 130 MW to 30 MW, equating to approximately 45.3 t/h of standard coal consumption.

The SGS provides the energy release mode in Case 4 for additional power output. When at peak power consumption, the unit is operated at the rated power of Case 1. The condensate and hot molten salt are arranged in a counterflow arrangement, as shown in Fig. 4. The hot salt passes through the superheater, evaporator and pre-heater before becoming cold salt, and the condensate conversely becoming superheated steam to the cold end of the reheater. In the end, the SGS

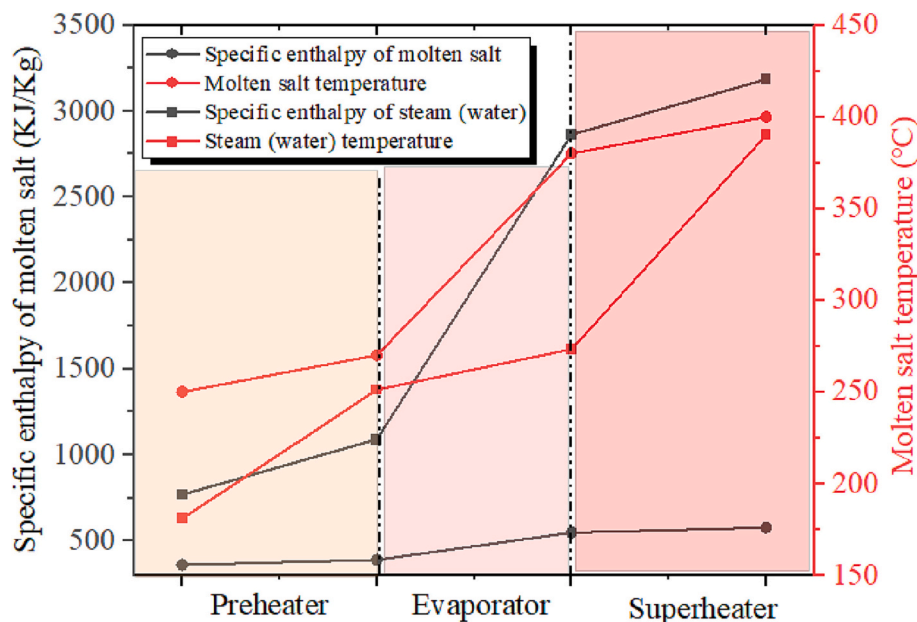


Fig. 4. Main parameters of the heat release process.



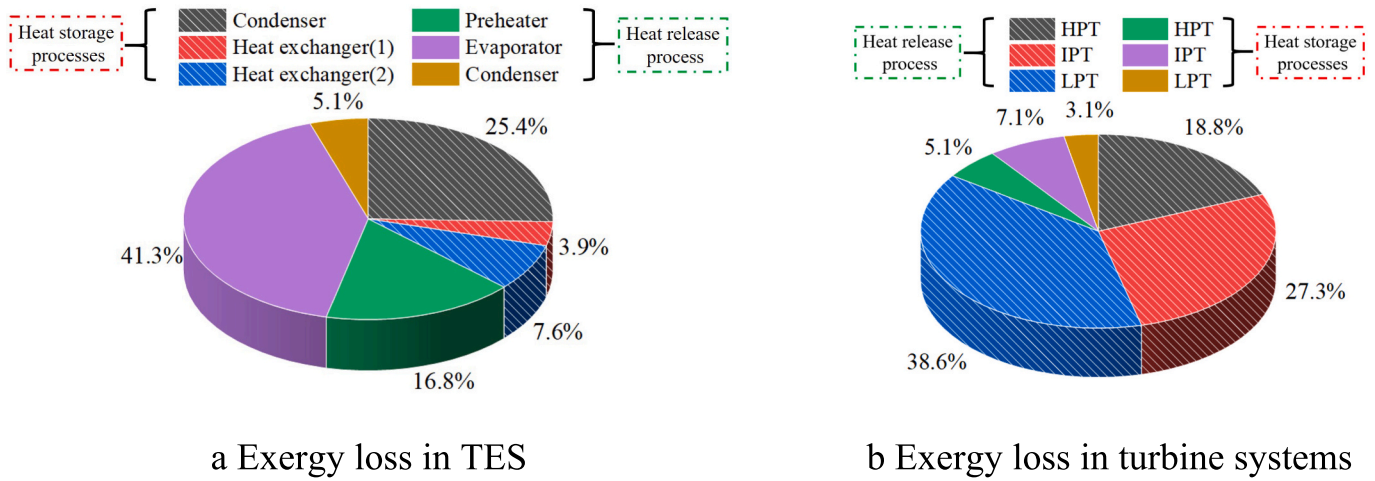


Fig. 7. TES and turbine exergy loss distribution.

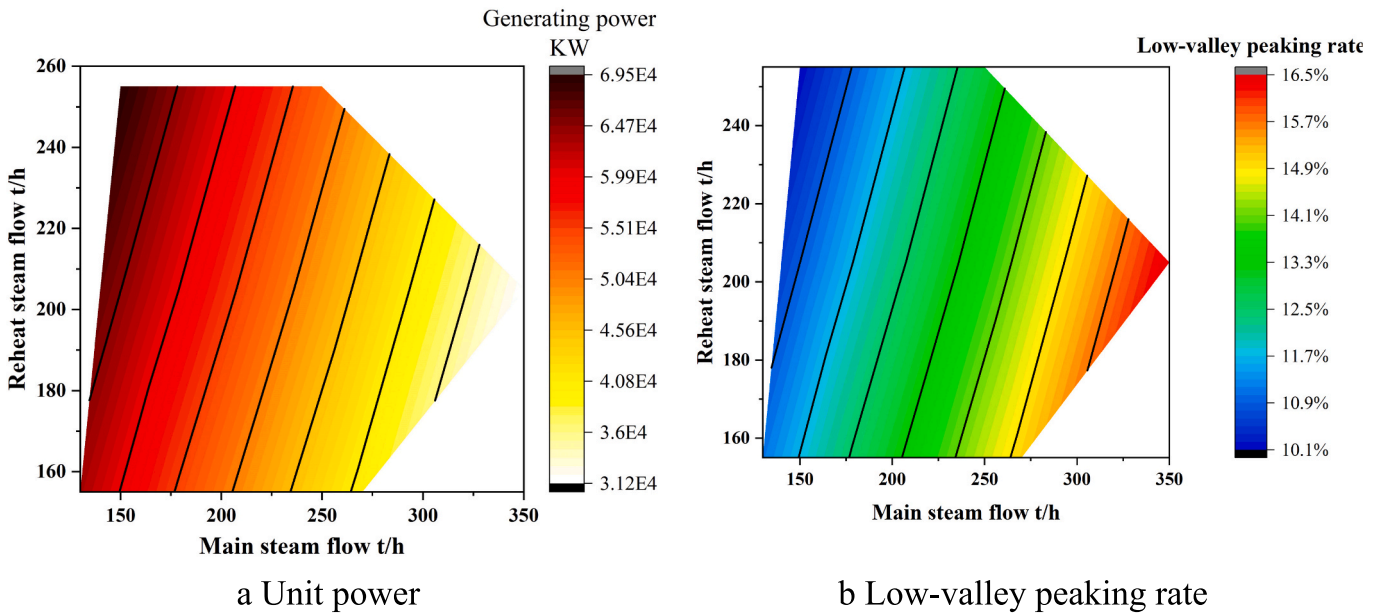


Fig. 8. Unit power generation and LVR for thermal storage processes.

opposite trend to the effect of the EMS. The authors concluded that with a fixed EMS, increasing the ERS leads to a higher EMS entering the steam ejector. A lower EMS going to the condenser leads to an increase in superheated steam returning to the cold end of the reheater, increasing the power generated by the system.

Further analysis shows that the LVR distribution of the unit is the same as the unit power distribution, with the higher EMS resulting in a significantly higher LVR of up to 16.5 %, which is significantly higher than the LVR reported in the literature. Several academics have proposed systems with a peaking rate distribution between 7 % and 15.5 %. [4,16,29,30] The high LVR indicates the superiority of TPSE in retrofitting thermal units, mainly because the retrofit system uses steam ejectors to mix the main steam and reheat steam back to the reheater again, solving the critical problem of reheater over-temperature. As shown in Fig. 9.a, the heat consumption rate varies considerably with the EMS, but is not significantly linked to the ERS. As the EMS rises from 150 to 350 t/h, the heat consumption rate becomes twice as high at approximately 40,000 kJ/kWh, mainly because more energy is stored in the TES and the power generation efficiency is reduced. The equivalent standard coal consumption does not show a clear pattern of variation

with EMS and ERS, but two peaks worth noting, a medium ERS with a low and medium EMS leading to an increase in coal consumption of approximately 7 t/h.

It is important to note that the valve opening at the cold salt tank outlet and the molten salt temperature after the first heat exchange stage (ITMS) are essential points of concern. As the mixing of main steam and superheated steam in different states also gives the same mixture of steam, resulting in multiple feasible solutions for the same operating condition. It has been found that the various feasible solutions correspond to different molten salt flow allocations and ITMS. Adjusting the valve openings and ITMS allows the required molten salt flow to be adjusted within a specific interval. Increasing the amount of molten salt increases the output power of the heat release process while increasing the system cost investment, but decreasing the amount of molten salt decreases the additional unit output power of the heat release process while decreasing the system cost investment. The molten salt flow rate variation (MSFR) within the adjustable range has an opposite effect on the investment cost and the additional unit output power, so an in-depth study of the MSFR is necessary. Therefore, the effects of EMS, ERS and MSFR on the performance of TPSE are next explained in detail. As shown

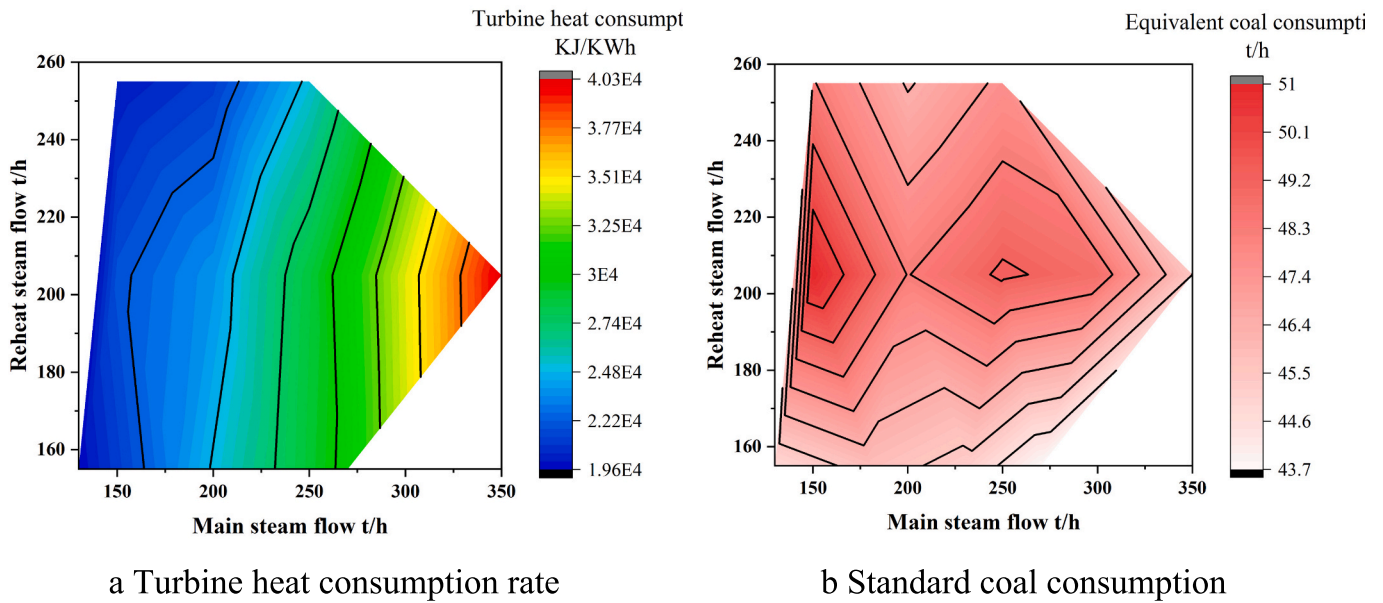


Fig. 9. Distribution of heat and coal consumption for thermal storage processes.

in Fig. 10.a, the molten salt flow rate (green bar) increases with EMS but decreases with ERS for the same reason as the unit power changes for the heat storage process. The maximum molten salt flow rate for the TPSE system at 16.5 % LVR is approximately 2600 t/h. Furthermore, different EMS and ERS do not correspond to the same MSAR (red bar), and the dominance of ERS allows the MSAR to expand. As mentioned earlier, the steam ejector is responsible for multiple feasible solutions for TPSE, but the strict guarantee that the three media at the inlet and outlet of the steam ejector are always in superheated steam allows for a range of feasible solutions for the system. The authors suggest that the dominance of ERS indicates a low EMS and that the main steam inlet of the steam ejector is most likely to experience condensation due to excessive heat exchange. Therefore, smaller EMS facilitates the regulation of heat exchange through valve opening and ITMS, leading to a larger MSAR. The MSAR for different extraction flows greatly affects the heat release power as shown in Fig. 10b. The pink color indicates the additional unit output power corresponding to the lowest molten salt flow rate for this

condition, while the green color indicates the additional unit output power increased by the MSAR. It can be seen that there is a clear positive correlation between the molten salt flow rate and the additional unit output power, with higher molten salt flow rates releasing more additional output power.

Further data processing as shown in Fig. 11a, LVR and PMR show the same trend as the extracted flow rate, with the PMR increasing significantly by 11.7 % as the EMS increases, but the ERS does not have a significant effect on the PMR. The authors concluded that the ERS completes the heat exchange with the molten salt through sensible heat only, while the specific enthalpy of the water vapor condensation process, as seen in Fig. 4, drops from 3250 to 750 kJ/kg, which is much greater than the heat exchange of sensible heat. Therefore, it is difficult for the ERS, which has not undergone condensation, to significantly impact the heat stored in the TES. Similarly, it is impossible to influence the PMR of the heat release process. Fig. 11b shows that MSAR positively affects unit power over the full range of extracted steam flow rates, with

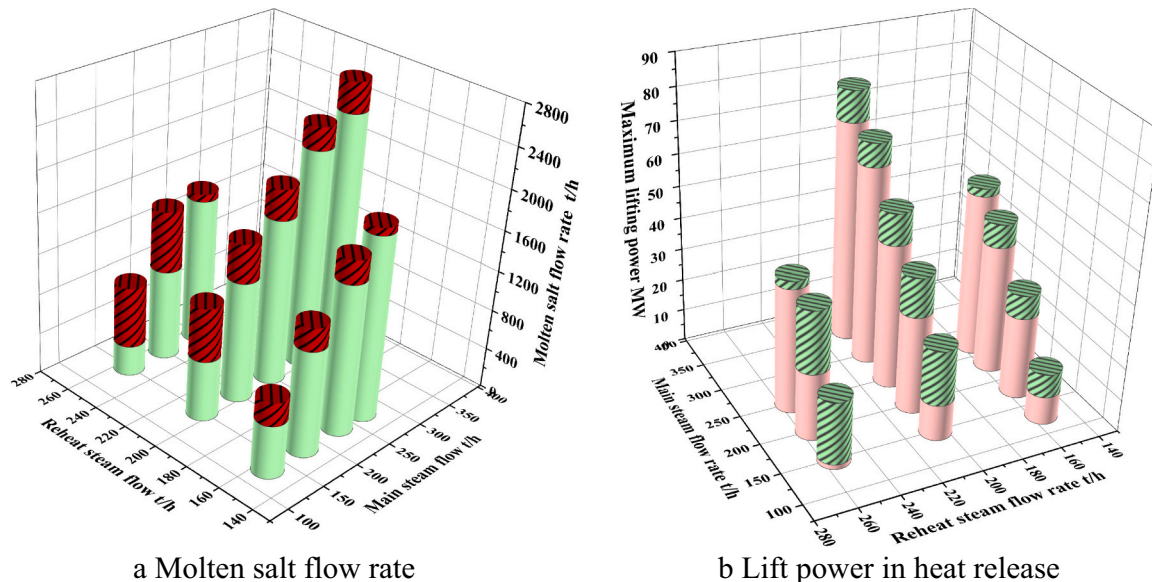


Fig. 10. Molten salt flow and additional output power for different extraction flow rates.

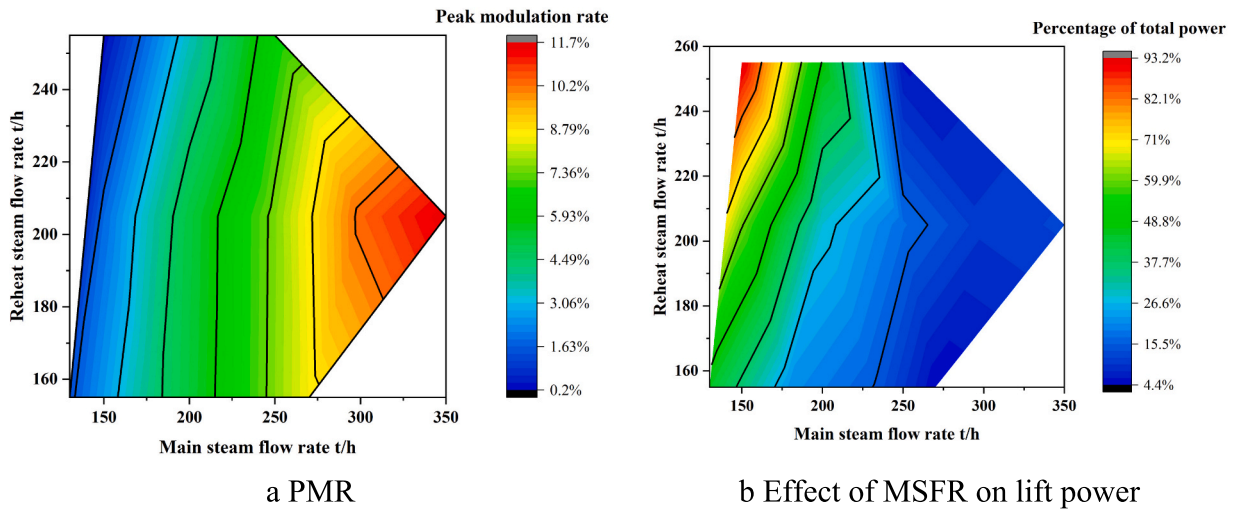


Fig. 11. PMR for different extraction flow rates; effect of MSAR on additional output power.

a significant percentage increase particularly in high ERS and low EMS conditions. Therefore, the operating range of ITMS and molten salt flow distribution ratios must be reasonably given to maximize corporate profits in engineering practice.

The cycle efficiency can be analyzed by unifying the heat storage and release processes, as can be seen in Fig. 12 where MSAR also affects the cycle efficiency of the system and the EMS dominates the change direction in the cycle efficiency of the system. As the EMS increases from 150 to 350 t/h, the cycle efficiency increases to about 80 %, which is higher than the known parameters reported in the literature. The effect of MSAR on cycling efficiency is shown in Fig. 12.c, which significantly increases cycling efficiency when ERS dominates. In summary, the TPES system can achieve LVR and PMR of 16.5 % and 11.7 %, respectively, while the 80 % cycle efficiency makes the TPSE market competitive. Multiple research has proposed cycle efficiencies of approximately 41.8 % to 69.88 % for TES-coupled thermal units, which is lower than the cycle efficiency of TPSE [28,30,31]. Zhang et al. based on a molten salt thermal storage system integrated with multiple heat sources (high-temperature flue gas and superheated steam) in a coal-fired power plant, with a TES cycle efficiency of 85.17 % [4]. In addition, introducing steam ejectors allows for more feasible solutions to the TPSE system, and the resulting MSAR provides significant optimization guidance for operating conditions where ERS dominates.

### 3.3. Effect of induced pressure on the system

The appropriate steam ejector has an essential impact on the stable operation of the system. The working medium in the steam ejector for this work is 11.9 MPa main steam, which can be suitably depressurized to achieve safe and stable operation of the TPSE system, depending on the actual steam ejector’s piloting capacity. Therefore, it is important to study the inlet pressure of the working medium of the steam ejector. As

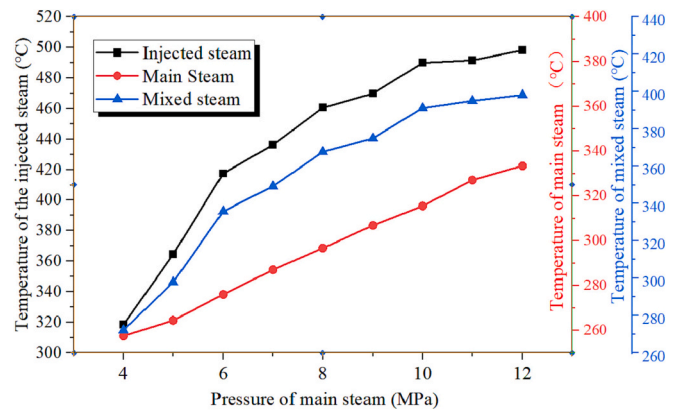


Fig. 13. Effect of ejector inlet pressure on temperature.

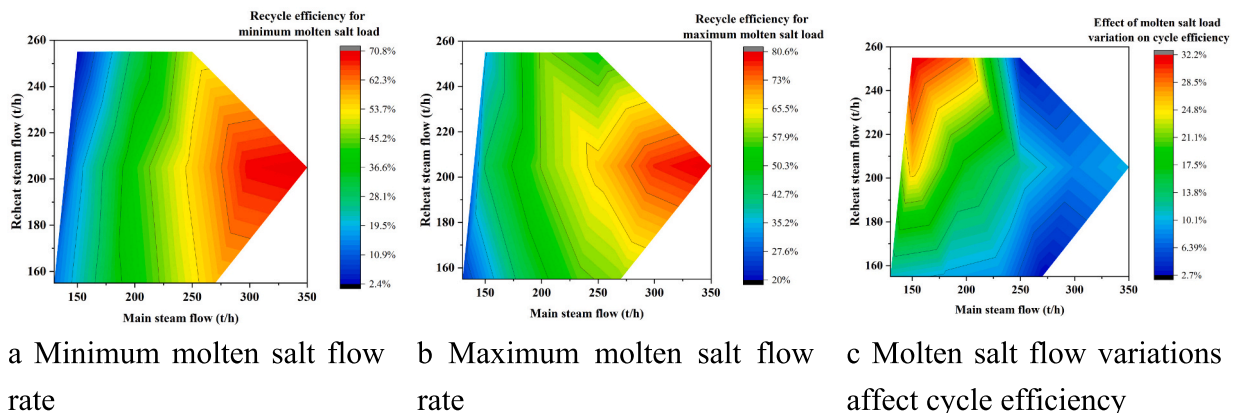


Fig. 12. Effect of different extraction flow rates and molten salt flow rates on cycle efficiency.

shown in Fig. 13, as the main steam pressure rises, the temperature of both the main steam and the reheated steam is diverted, resulting in the outlet mixture rising from 290 °C to approximately 390 °C. It is worth noting that too high or too low outlet temperature can lead to either too high or too low outlet temperature of the reheater, which can affect the safe operation of the system. Fig. 13 clarifies the relationship between inlet pressure and steam outlet temperature, providing a direction of adjustment for safe system operation. Also, Fig. 14 shows that the EMS and unit power generation decreases as the main steam pressure increases, but the injection coefficient increases to approximately 2.4. The increase in main steam pressure gives it a higher induced capacity, which drives up the injection coefficient. The increased injection coefficient results in lower main steam flow to the steam ejector and more main steam going to the TES, which leads to a reduction in the power output of the heat storage process. Fig. 15 shows how the unit peaking molten salt flow rate and LVR varies with the main steam pressure. Higher main steam pressures result in lower system output power and higher LVR. At the same time, the introduced unit peak molten salt flow rate indicates the molten salt flow rate required to regulate 1 % of the unit's power output depth, reflecting the ease of system regulation. High main steam pressure causes the unit peaking molten salt flow rate to drop from 100 t/h to 90 t/h, reducing the difficulty of the system peak. In summary, the inlet pressure of the main steam should be increased within the permissible range of mechanical manufacturing capacity, which can improve the LVR of the system and the molten salt flow rate per unit peaking depth, which is of great significance for the operation of TPSE.

### 3.4. Economic analysis

The technical feasibility of the TPSE system has been described in detail earlier, but it is not only the technology that determines whether a coupled system is competitive in the marketplace but also the investment cost and payback period of the system that needs to be considered. Payback within a suitable number of years and sustained profitability are the core competencies of a new system. This work uses the NPV method to compare the cumulative profit change process of the original thermal power plant system and TPSE to ensure the reasonableness of the economic calculation. Table 2 below gives the infrastructure costs and main parameters of TPSE. Since the capacity and volume of the salt tank affect the peak shaving capacity and economic cost, the specific parameters of the salt tank and molten salt are given in this work based

on the actual conditions in the field as shown in Table 3. Based on the results discussed earlier, a TES with a storage power of 70 MW and a peaking duration of 6 h in a cycle would require 420 MWh of TES to be built. Current data from the China Electricity Council shows that the cost per kWh of peaking capacity for thermal power unit flexibility conversion is around RMB 500 to RMB 1500. The investment cost for this work is RMB 218 million, with an average peaking construction cost of RMB 520 for a kWh [28], making the cost reasonable. The following is a calculation of the annual net cash flow based on the NPV, which is the sum of the costs occurring in the future, discounted at a certain discount rate (discount rate), to the value of the investment in the first year, where the costs occurring in the future include the annual expenditure and revenue. The TPSE payback is calculated as in Eq. (16), where  $N_{\text{cycle}}$  indicates the number of TPSE peaking cycles per year,  $i_0$  indicates the market benchmark discount rate,  $n$  is the number of years of TPSE operation, and  $t$  indicates the year of calculation.  $NPV(n) = 0$  indicates that the payback is complete in year  $n$ , and greater than and  $<0$  indicate the start of profit and loss, respectively.

$$NPV(n) = \sum_{t=0}^{n-1} C_{\text{cycle}} N_{\text{cycle}} (1 + i_0)^{-t} \quad (16)$$

As seen from the base case in Fig. 16.a, the TPSE system starts to make a profit in 3.8 years and has sustained profitability of up to RMB 25 million/year when the five-year bank loan is completed. TPSE system is not only technically feasible but also has reasonable economic indicators and is a product with significant market competitiveness. In order to clarify the impact of the main economic parameters on the stability of the system, Fig. 16 shows the impact of TPSE running time and market benchmark discount rate on NPV. It can be seen that a 10 % and 20 % change in interest rates has a small impact on NPV, indicating that the external financial environment does not have a serious impact on TPSE. However, a 10 % and 20 % change in operating hours seriously impact the profitability of the system, with a 10 % reduction in system operating hours resulting in an extended payback period of 4.8 years. Therefore, ensuring effective peaking times is essential for the stable operation of TPSE systems.

In addition, an economic analysis was carried out for different discount factors to assess the applicability of TPSE in different regions. As can be seen in Fig. 16b, the discount factor has a significant impact on the NPV, with a  $u$  of 0.2 indicating that there are no significant peaks and valleys in the region and that TPSE is not necessary, making it difficult for the system to complete capital recovery in the short term. An

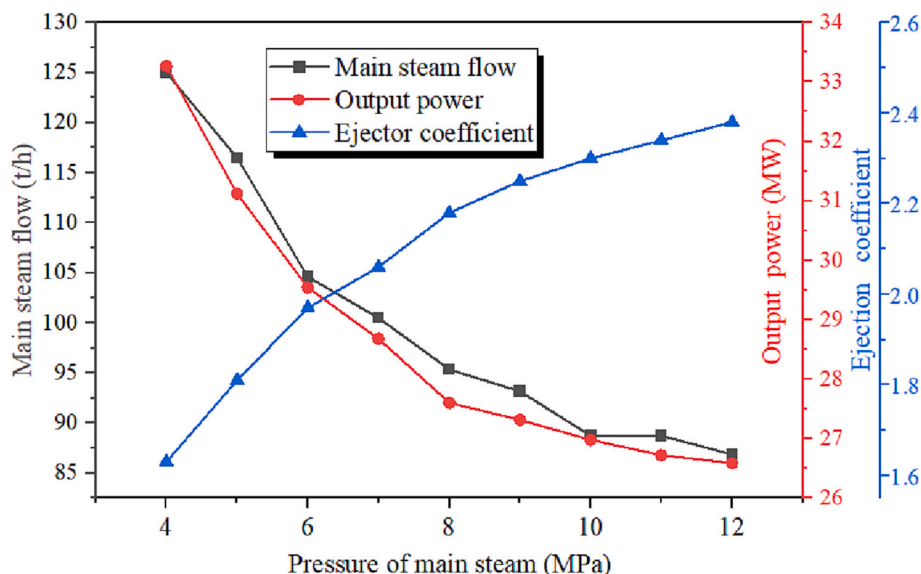


Fig. 14. Effect of ejector inlet pressure on main steam flow, output power and ejection coefficient.

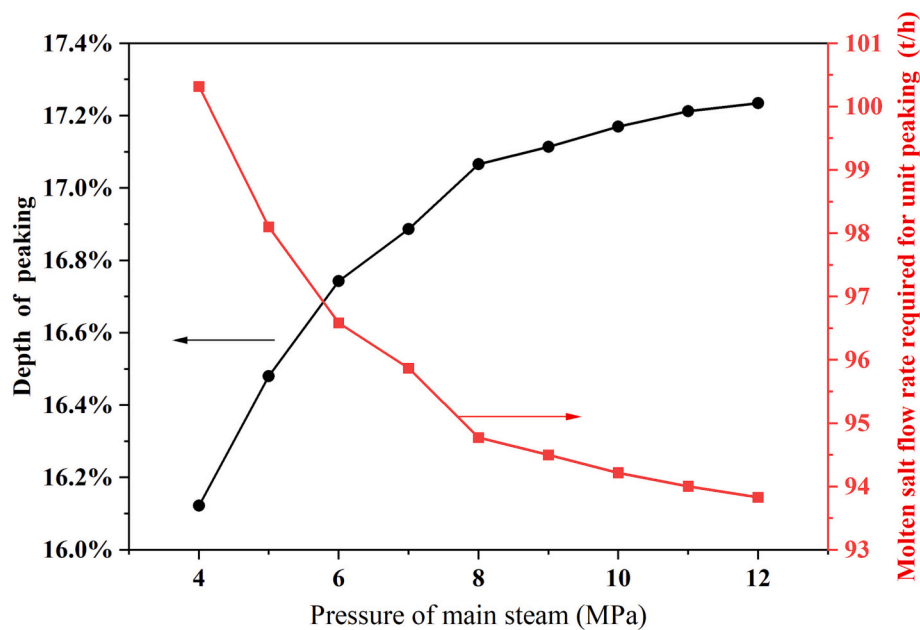


Fig. 15. Effect of ejector inlet pressure on LVR and unit peaking molten salt flow rate.

Table 2

Economic analysis parameters.

Component	Ternary salt [28]	Salt tank [28]	Heat exchanger [32,33]	Ejector	Pump, etc. [32,33]	Construction [32,33]	DCS
Cost/million	49	40	31	8.6	32.2	37.2	20
Component	$i_0$	Loan ratio	Loan term y	Peak hours	Peaking cycle of a year	u	Maintenance million
Value	5 %	45 %	5	6	300	0.3	5

Table 3

the specific parameters of the salt tank and molten salt.

Salt tank		Molten salt	
Material of hot salt tank	S31603 (316L)	Composition of molten salt (Hetic)	53 % $\text{KNO}_3$ -40% $\text{NaNO}_2$ -7% $\text{NaNO}_3$
Material of cold salt tank	Carbon steel	Operating temperature range	220 °C-430 °C
Cost	316L (200000RMB/t) Carbon steel (3700RMB/t)	Cost	11200RMB/t

u of 0.3 indicates some peak and valley separation of electricity prices in the area, that the TPSE system can complete payback in four years and that TPSE has a presence. Take the Chinese region as an example, the low valley tariff in Shanghai is about RMB 0.3/kWh and the average peak tariff is about RMB 1.1, which corresponds to a discount factor u of 0.4; the low valley tariff in Anhui is about RMB 0.45/kWh and the average peak tariff is about RMB 0.95, which corresponds to a discount factor u of 0.25. A TPSE project in Shanghai takes only 2 years to recover capital, but it takes about 6 to 7 years in Anhui. Therefore, constructing a TPSE requires a detailed calculation of the discount factor for each region to ensure that the capital recovery will be completed.

The above discussion is based on taking 205 t/h and 350 t/h for ERS and EMS, but the operation may be adjusted for the extraction flow rate. Fig. 17 shows the payback period for different extraction flow rates, assuming a discount factor u of 0.3, with the investment cost scaled equally according to the storage capacity of the TES and the remaining parameters kept in line with Table 2. It can be seen that the EMS significantly influences the payback years and not so much by the ERS,

similar to the distribution of LVR and PMR for TPSE, the main reasons for which have been discussed earlier. It is worth noting that the ERS and EMS are distributed in a circular pattern, indicating that two different ERSs will exist to achieve the same payback year for the same EMS, which provides a variety of possibilities for the selection of practical operating solutions. In addition, when the EMS is <250 t/h the payback time of the system will exceed 15 years, at which point it may be challenging to meet the economic viability of the TPSE.

#### 4. Conclusion

The random, fluctuating and intermittent characteristics of the fast-growing new energy generation challenge large-scale grid connections and place higher demands on the peaking and consumption capacity of the grid. In order to further improve the regulation capability of the thermal power unit system, this work proposes a new thermal power unit peaking system coupled with TES and steam ejector. New retrofit system is proved to be technically and economically feasible based on the simulation of a 600 MW thermal power unit.

- (1) Results show that the percentage of exergy losses in the retrofitted system is in the order of condenser, turbine and TES, with the exergy losses in the heat release process accounting for approximately 70 % of the cycle. The key equipment of the turbine exergy loss is the medium-pressure and low-pressure turbine in heat storage and release process, respectively. The condenser and evaporator corresponding to the storage and heat processes are the main components of the TES exergy losses, accounting for 60 % of the total TES exergy losses.
- (2) The retrofitted system has a maximum cycle efficiency of 70–80 % and peak-valley regulation rate of 16.5 % and 11.7 %, higher than the current thermal unit retrofit system. Further research

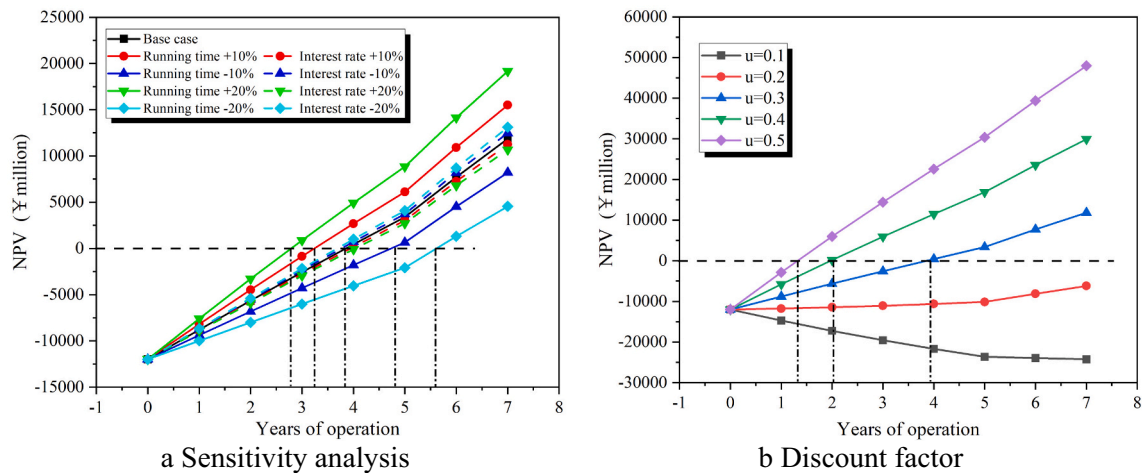


Fig. 16. Economic sensitivity analysis of TPSE and the impact of the discount factor on NPV.

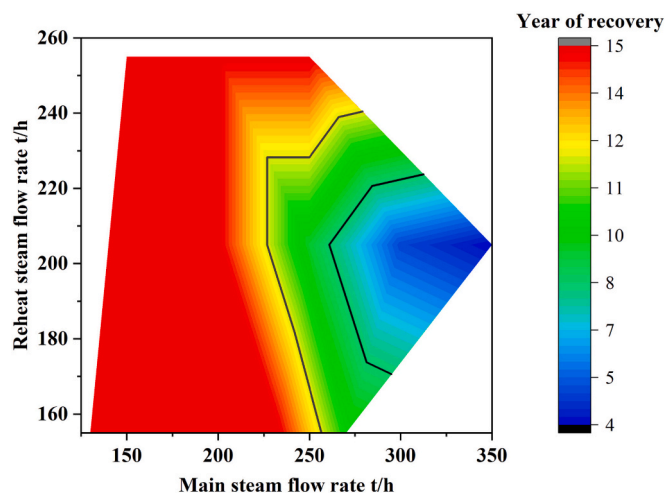


Fig. 17. Effect of different extraction flows for TPSE on recovery life.

has found that extraction of main steam dominates the peaking rate and cycling efficiency compared to extraction of reheat steam. In addition, molten salt flow rate variation has a significant impact on high ERS systems that must be considered. Increasing the main steam pressure at the ejector inlet increases the valley regulation rate by 1.5 %, while reducing the molten salt flow rate per unit peaking depth by 10 t/h, which is essential for the stable operation of the retrofitted system.

- (3) The economic analysis of the retrofitted system shows that the system operating time is the main factor affecting the payback period compared to the discount rate. The regional tariff discount factor significantly impacts the retrofitted system, which will not be economically viable when  $u < 0.2$ . The economic analysis of the base case shows that the retrofitted system starts to be profitable in 3.8 years, with later profitability of up to RMB 25 million/year. Further analysis reveals that two different extractions of reheat steam with the same extraction of main steam will achieve the same payback period, which offers a variety of possibilities for practical operational scenarios. In addition, when the extraction of main steam is  $< 250$  t/h the payback time of the system will exceed 15 years, at which point it will be difficult to meet the economic viability of the retrofitted system.

### CRediT authorship contribution statement

**Xiang Liu:** Conceptualization, Writing – review & editing, Visualization, Supervision. **Kelang Jin:** Formal analysis, Investigation, Data curation. **Xue Xue:** Methodology, Software, Validation. **Lei Zhang:** Formal analysis. **Hao Zhou:** Project administration, Funding acquisition, Formal analysis, Investigation.

### Declaration of competing interest

The authors declare that they have no known competing financial interests or personal relationships that could have appeared to influence the work reported in this paper.

### Data availability

Data will be made available on request.

### Acknowledgements

Supported by the Fundamental Research Funds for the Central Universities (2022ZFJH04). Also, many thanks to Binquan Wang for his help with the modeling work in this paper.

### References

- [1] O. Pupo-Roncallo, J. Campillo, D. Ingham, K. Hughes, M. Pourkashanian, Large scale integration of renewable energy sources (RES) in the future Colombian energy system, *Energy* 186 (2019), 115805, <https://doi.org/10.1016/j.energy.2019.07.135>.
- [2] J. Yang, Y. Li, H. Tan, J. Bian, X. Cao, Optimization and analysis of a hydrogen liquefaction process integrated with the liquefied natural gas gasification and organic Rankine cycle, *J. Energy Storage* 59 (2023), 106490, <https://doi.org/10.1016/j.est.2022.106490>.
- [3] X. Fan, W. Ji, L. Guo, Z. Gao, L. Chen, J. Wang, Thermo-economic analysis of the integrated system of thermal power plant and liquid air energy storage, *J. Energy Storage* 57 (2023), 106233, <https://doi.org/10.1016/j.est.2022.106233>.
- [4] T. Ouyang, P. Qin, S. Xie, X. Tan, M. Pan, Flexible dispatch strategy of purchasing-selling electricity for coal-fired power plant based on compressed air energy storage 267 (2023) 126578.
- [5] H. Ibrahim, A. Ilinca, J. Perron, Energy storage systems—characteristics and comparisons, *Renew. Sust. Energ. Rev.* 12 (2008) 1221–1250, <https://doi.org/10.1016/j.rser.2007.01.023>.
- [6] E. Borri, A. Tafone, G. Zsembinszki, G. Comodi, A. Romagnoli, L.F. Cabeza, Recent trends on liquid air energy storage: a bibliometric analysis, *Appl. Sci.* 10 (2020) 2773.
- [7] P. Eser, A. Singh, N. Chokani, R.S. Abhari, Effect of increased renewables generation on operation of thermal power plants, *Appl. Energy* 164 (2016) 723–732.
- [8] S.Ó. Garðarsdóttir, L. Göransson, F. Normann, F. Johnsson, Improving the flexibility of coal-fired power generators: impact on the composition of a cost-optimal electricity system, *Appl. Energy* 209 (2018) 277–289.

- [9] D. Li, Y. Hu, D. Li, J. Wang, Combined-cycle gas turbine power plant integration with cascaded latent heat thermal storage for fast dynamic responses, *Energy Convers. Manag.* 183 (2019) 1–13, <https://doi.org/10.1016/j.enconman.2018.12.082>.
- [10] Y. Zhao, J. Song, M. Liu, Y. Zhao, A.V. Olympios, P. Sapin, J. Yan, C.N. Markides, Thermo-economic assessments of pumped-thermal electricity storage systems employing sensible heat storage materials, *Renew. Energy* 186 (2022) 431–456, <https://doi.org/10.1016/j.renene.2022.01.017>.
- [11] V.D. Stevanovic, M.M. Petrovic, S. Milivojevic, M. Ilic, Upgrade of the thermal power plant flexibility by the steam accumulator, *Energy Convers. Manag.* 223 (2020), 113271, <https://doi.org/10.1016/j.enconman.2020.113271>.
- [12] A.A. Al Kindi, M. Aunedi, A.M. Pantaleo, G. Strbac, C.N. Markides, Thermo-economic assessment of flexible nuclear power plants in future low-carbon electricity systems: role of thermal energy storage, *Energy Convers. Manag.* 258 (2022) 115484, <https://doi.org/10.1016/j.enconman.2022.115484>.
- [13] M. Johnson, J. Vogel, M. Hempel, A. Dengel, M. Seitz, B. Hachmann, High temperature latent heat thermal energy storage integration in a co-gen plant, *Energy Procedia* 73 (2015) 281–288, <https://doi.org/10.1016/j.egypro.2015.07.689>.
- [14] S. Guo, *Model Based Analysis of Power Plant Integrated With a Post Combustion Carbon Capture Process*, University of Warwick, 2015.
- [15] M. Draganescu, *Study of Supercritical Coal-Fired Power Plant Dynamic Responses and Control for Grid Code Compliance*, University of Warwick, 2015.
- [16] D. Li, J. Wang, Study of supercritical power plant integration with high temperature thermal energy storage for flexible operation, *J. Energy Storage* 20 (2018) 140–152, <https://doi.org/10.1016/j.est.2018.09.008>.
- [17] J.D. Wojcik, J. Wang, Technical feasibility study of thermal energy storage integration into the conventional power plant cycle, *Energies* 10 (2017) 205.
- [18] B.M. Tashtoush, M.d.A. Al-Nimr, M.A. Khasawneh, A comprehensive review of ejector design, performance, and applications, *Appl. Energy* 240 (2019) 138–172, <https://doi.org/10.1016/j.apenergy.2019.01.185>.
- [19] Y. Xue, Z. Ge, L. Yang, X. Du, Peak shaving performance of coal-fired power generating unit integrated with multi-effect distillation seawater desalination, *Appl. Energy* 250 (2019) 175–184, <https://doi.org/10.1016/j.apenergy.2019.04.190>.
- [20] Y. Zhang, N. Xiong, Z. Ge, Y. Zhang, J. Hao, Z. Yang, A novel cascade heating system for waste heat recovery in the combined heat and power plant integrating with the steam jet pump, *Appl. Energy* 278 (2020), 115690.
- [21] J. Peng, G. Lu, L. Song, T. Li, Performance study on the geothermal bypass injection-organic rankine cycle power generation system, *Proc. Chin. Soc. Electr. Eng.* 36 (2016) 5300–5307, <https://doi.org/10.13334/j.0258-8013.pcsee.150793>.
- [22] R. Beebe, Condition monitoring of steam turbines by performance analysis, *J. Qual. Maint. Eng.* 9 (2003) 102–112, <https://doi.org/10.1108/13552510310482361>.
- [23] W. Chen, M. Liu, D. Chong, J. Yan, A.B. Little, Y. Bartosiewicz, A 1D model to predict ejector performance at critical and sub-critical operational regimes, *Int. J. Refrig.* 36 (2013) 1750–1761, <https://doi.org/10.1016/j.ijrefrig.2013.04.009>.
- [24] R. Liu, Y. Wang, P. Fan, M. Liu, Performance analysis of a heat power synergy system integrated with steam ejectors under the full working condition, *J. Chin. Soc. Power Eng.* 43 (2023) 56–64.
- [25] K. Zhang, M. Liu, Y. Zhao, H. Yan, J. Yan, Design and performance evaluation of a new thermal energy storage system integrated within a coal-fired power plant, *J. Energy Storage* 50 (2022), 104335, <https://doi.org/10.1016/j.est.2022.104335>.
- [26] B. Wang, H. Ma, S. Ren, F. Si, Effects of integration mode of the molten salt heat storage system and its hot storage temperature on the flexibility of a subcritical coal-fired power plant, *J. Energy Storage* 58 (2023), 106410, <https://doi.org/10.1016/j.est.2022.106410>.
- [27] Z. Yao, C. Romero, J. Baltrusaitis, Combustion optimization of a coal-fired power plant boiler using artificial intelligence neural networks, *Fuel* 344 (2023), 128145, <https://doi.org/10.1016/j.fuel.2023.128145>.
- [28] Q. Yong, Y. Tian, X. Qian, X. Li, Retrofitting coal-fired power plants for grid energy storage by coupling with thermal energy storage, *Appl. Therm. Eng.* 215 (2022), 119048, <https://doi.org/10.1016/j.applthermaleng.2022.119048>.
- [29] M. Richter, G. Oeljeklaus, K. Görner, Improving the load flexibility of coal-fired power plants by the integration of a thermal energy storage, *Appl. Energy* 236 (2019) 607–621, <https://doi.org/10.1016/j.apenergy.2018.11.099>.
- [30] K. Zhang, M. Liu, Y. Zhao, S. Zhang, H. Yan, J. Yan, Thermo-economic optimization of the thermal energy storage system extracting heat from the reheat steam for coal-fired power plants, *Appl. Therm. Eng.* 215 (2022), 119008, <https://doi.org/10.1016/j.applthermaleng.2022.119008>.
- [31] R. Cao, Y. Lu, D. Yu, Y. Guo, W. Bao, Z. Zhang, C. Yang, A novel approach to improving load flexibility of coal-fired power plant by integrating high temperature thermal energy storage through additional thermodynamic cycle, *Appl. Therm. Eng.* 173 (2020) 15225, <https://doi.org/10.1016/j.applthermaleng.2020.115225>.
- [32] F. Schöniger, R. Thonig, G. Resch, J. Lilliestam, Making the sun shine at night: comparing the cost of dispatchable concentrating solar power and photovoltaics with storage, *Energy Sources B* 16 (2021) 55–74, <https://doi.org/10.1080/15567249.2020.1843565>.
- [33] M. Mehos, C. Turchi, J. Vidal, M. Wagner, Z. Ma, C. Ho, *Concentrating Solar Power Gen3 Demonstration Roadmap*, United States, 2017.